The Chloroalkoxide Route to Transition Metal Oxides. Synthesis of V_2O_5 Thin Films and Powders from a Vanadium Chloromethoxide

Mauro Epifani,*[,†] Teresa Andreu,[‡] Carlos R. Magana,[§] Jordi Arbiol,[§,||] Pietro Siciliano,[†] Massimiliano D'Arienzo,[⊥] Roberto Scotti,[⊥] Franca Morazzoni,[⊥] and Joan R. Morante[‡,#]

Consiglio Nazionale delle Ricerche − Istituto per la Microelettronica ed i Microsistemi (C.N.R.-I.M.M.), via Monteroni, I-73100 Lecce, Italy, M2E-IN2UB, Department of Electrònica, Universitat de Barcelona, C. Martí i Franquès 1, 08028 Barcelona, CAT, Spain, MIND-IN2UB, Department of Electrònica, Universitat de Barcelona, C. Martí i Franquès 1, 08028 Barcelona, CAT, Spain, TEM-MAT, Serveis Cientificotecnics, Universitat de Barcelona, 08028 Barcelona, CAT, Spain, Dipartimento di Scienza dei Materiali, Università degli Studi di Milano-Bicocca, via R. Cozzi 53, 20125 Milano, Italy, and Institut de Recerca en Energia de Catalunya (IREC), C/Josep Pla 2, 08019 Barcelona, Spain

Received December 2, 2008. Revised Manuscript Received February 24, 2009

Vanadium chloromethoxide was prepared by the methanolysis of VCl_4. The addition of water with a H_2O:vanadium molar ratio ranging between 0 and 16 changed the solution color from green to deep blue at a rate increasing with water concentration. UV−vis, Fourier transform infrared, Raman, and electron paramagnetic resonance spectroscopy investigations showed that VCl_4 precursor is initially methanolyzed to $(VO)Cl_x(OCH_3)_y$ ($x + y = 4$) monomers. Upon water addition, methoxo ligands undergo hydrolysis. The presence of chlorine ligands and of the vanadyl group explains the long-term stability of the solutions. V_2O_5 thin films and powders were prepared, respectively, by spin-coating onto silicon substrates and drying of the solutions, followed by heat-treatments at temperatures up to 500 °C. Films and powder precursors were characterized by X-ray diffraction, FTIR, Raman, UV−vis, and EPR spectroscopy, transmission electron microscopy, and thermal analyses. The structural evolution begins by condensation of the initial monomers to form amorphous structures with poor extension of the three-dimensional network. Heat-treatment at higher temperatures induces further condensation and the elimination of the chlorine ligands, which leave an oxygen-defective structure and cause the initial formation of substoichiometric V_3O_7 phase. When the samples were annealed at $T \geq 400$ °C, only the V_2O_5 phase was found. V_2O_5 powders annealed at 500 °C were used in chemoresistive gas sensing devices and were able to detect reducing gases such as ammonia and ethanol over a broad range of concentrations by stable and reliable signal.

Introduction

Metal alkoxides[1] are a versatile class of precursors for the synthesis of metal oxide materials, through solvolytic reactions known as sol−gel process. Alkoxides are known for a large number of elements and are easily available for technologically relevant elements like Ti and Zr. Si alkoxides are taking on an overwhelming importance for their versatile use in the synthesis of functionalized silica structures.[2] Apart from these notable exceptions, in general, metal alkoxides suffer from some limitations in their use due to high cost, high reactivity to even traces of moisture, and limited time stability. For this reason, alternative oxide precursors have been exploited. An example is the use of vanadates in the synthesis of V_2O_5[3] instead of vanadyl alkoxides:[4] the vanadates are easily available, and their tendency to inorganic polymerization was very well-known.[5] These favorable conditions of course cannot be expected for all elements, so the development of a whole general class of precursors alternative to metal alkoxides is of interest. These precursors should solve some of the problems of the processing of metal alkoxides, while at the same time retaining important features such as the hydrolytic processing. A class of precursors with

* To whom correspondence should be addressed. E-mail: mauro.epifani@le.imm.cnr.it.
† C.N.R.-I.M.M.
‡ M2E-IN2UB, Universitat de Barcelona.
§ MIND-IN2UB, Universitat de Barcelona.
|| Serveis Cientificotecnics, Universitat de Barcelona.
⊥ Università degli Studi di Milano-Bicocca.
IREC.

(1) (a) Bradley, D. C.; Mehrothra, R. C.; Gaur, D. P. *Metal Alkoxides*; Academic Press: London, UK, 1978. (b) Turova, N. Y., Turevskaya, E. P., Kessler, V. G., Yanovskaya, M. I., Eds. *The Chemistry of Metal Alkoxides*; Springer: Heidelberg, Germany, 2002.
(2) (a) Bagwe, R. P.; Hilliard, L. R.; Tan, W. *Langmuir* **2006**, *22*, 4357–4362. (b) Trewin, B. G.; Slowing, I. I.; Giri, S.; Chen, H.-T.; Lin, V. S.-Y. *Acc. Chem. Res.* **2007**, *40*, 846–853. (c) Margelefsky, E. L.; Bendjeriou, A.; Zeidan, R. K.; Dufaud, V.; Davis, M. E. *J. Am. Chem. Soc.* **2008**, *130*, 13442–13449. (d) Kim, J.-H.; Bryan, W. W.; Lee, T. R. *Langmuir* **2008**, *24*, 11147–11152. (e) Sankaraiah, S.; Min Lee, J.; Kim, J. H.; Choi, S. W. *Macromolecules* **2008**, *41*, 6195–6204.
(3) (a) Livage, J. *Chem. Mater.* **1991**, *3*, 578–593. (b) Livage, J. *Solid State Ionics* **1996**, *86−88*, 935–942. (c) Livage, J. *Coord. Chem. Rev.* **1998**, *178−180*, 999–1018. (d) Bouhedja, L.; Steunou, N.; Maquet, J.; Livage, J. *J. Solid State Chem.* **2001**, *162*, 315–321.
(4) (a) Partlow, D. P.; Gurkovich, S. R.; Radford, K. C.; Denes, L. J. *J. Appl. Phys.* **1991**, *70*, 443–452. (b) Stiegman, A. E.; Eckert, H.; Plett, G.; Kim, S. S.; Anderson, M.; Yavrouian, A. *Chem. Mater.* **1993**, *5*, 1591–1594. (c) Chaput, F.; Dunn, B.; Fuqua, P.; Salloux, K. *J. Non-Cryst. Solids* **1995**, *188*, 11–18. (d) Ozer, N. *Thin Solid Films* **1997**, *305*, 80–87. (e) Klett, U.; Fricke, J. *J. Non-Cryst. Solids* **1998**, *238*, 45–50.
(5) Lemerle, J.; Nejem, L.; Lefebvre, J. *J. Inorg. Nucl. Chem.* **1982**, *42*, 17–20. See also the historical account in ref 3a.

10.1021/cm803242m CCC: $40.75
Published on Web 03/25/2009

such characteristics emerges when considering, among the routes to synthesize metal alkoxides, the solvolysis of anhydrous metal chlorides,[1] which is known for a broad range of elements such as Sn, Ti, Zr, Si, Mo, V, W, Hf, etc. In previous works on the synthesis of SnO_2[6] and MoO_3,[7] we have observed that if the purification steps necessary to remove the residual chlorine in the alkoxide synthesis are omitted, intermediate precursors are obtained, which have the general formula of a chloroalkoxide: $MCl_x(OR)_y$. In fact, the Sn and Mo chloroalkoxides displayed remarkable time stability and could be easily processed even in the presence of moisture to provide thin films and powders. On the other hand, the residual chlorine was eliminated during the heat-treatments to prepare the final materials. It then seemed of interest to continue the investigation of this class of precursors, to establish the applicability and the disadvantages in comparison with pure alkoxides. In this work, we present the synthesis of a vanadium chloromethoxide from methanolysis of VCl_4, and its successful application in the synthesis of V_2O_5 thin films and powders. The investigation, carried out by combining different spectroscopic techniques, showed that the remarkable time stability of the precursor solution is due to residual chlorine ligands and to the presence of the vanadyl group. The residual chlorine also has a role in determining the structural evolution of the precursor to the final films and powders, through the formation of intermediate, substoichiometric phases. Finally, we show the results of gas-sensing tests carried out with the prepared materials, where stable and reliable response to reducing gases like ammonia and ethanol was obtained.

While the focus of our work was the development of basic knowledge of the chloroalkoxides sol−gel chemistry, further potential application beyond gas sensors emerges when considering the wet chemical procedures developed in the past for the preparation of supported V_2O_5 catalysts. The catalysts were prepared by impregnation of a porous support with solution of various vanadates[8] and, in less common cases, alkoxides.[9] With respect to these procedures, the chloroalkoxides present some important advantages: as mentioned above, they are less expensive than alkoxides and easier to handle; above all, as we shall show in this Article, they easily form highly polymerized layers of oxide. This feature could decrease the possible segregation and poor coverage that may result from the use of vanadate solutions in impregnation procedures.

Experimental Section

VCl_4, methanol, and cetyltrimethylammonium bromide (CTAB) (Sigma-Aldrich) were used as received. Silicon substrates (⟨100⟩ orientation) with a 5000 Å SiO_2 overlayer were provided by ST Microelectronics. For methanolysis of VCl_4, 10 mL of MeOH was slowly added to 0.75 g of VCl_4 in a glovebox (Braun, LabStar) with $H_2O < 1$ ppm. A green solution was obtained, with evolution of green smoke. After the smoke evolution ceased, the solution was taken out of the glovebox, and water was added dropwise. The solution color immediately turned to darker green. Different H_2O:V molar ratios, denoted hereafter with r, were employed, ranging from 0 to 16. Only in the case of $r = 0$ was the solution directly sealed in a vial in the glovebox. Two weeks after water addition, the solution with $r = 16$ had become bright blue. Films and powders were prepared from the solutions with $r = 16$, because it enhanced the rate of color change of the solution and decreased the overall preparation time. For preparing thin films, 30 mg of CTAB was added to the solution, which after 1 day was spin-coated at 2000 rpm onto silicon substrates, precleaned for 2 min in boiling isopropanol. The films were dried for 3 min at 80 °C in air, then heat-treated for 1 h at temperatures ranging from 100 to 500 °C in air atmosphere in a tubular furnace, with a heating rate of 300 °C/h. The films were very uniform and crackless after the various heat-treatments. The thickness of a film heat-treated at 400 °C was about 110 nm, as measured by a profilometer (Tencor Instruments, Alpha-Step IQ). Powders were prepared from the sols by evaporating the solvent in a rotary evaporator, at a pressure decreased from 100 to 40 mbar in about 30 min and with the bath temperature raised from room temperature to 80 °C in about 1 h. The resulting dark, viscous product was further dried at 80 °C overnight in an air oven. The final product was heat-treated at various temperatures similarly to the thin films.

The green line ($\lambda = 514$ nm) of a Jobin Yvon T64000 spectrometer with an INNOVA 300 Coherent Ar laser and a bidimensional CCD detector cooled with liquid nitrogen was used for Raman analysis of the solutions and powders.

The Fourier transform infrared (FTIR) spectroscopic measurements were carried out on the solutions with a Bomem MB-120 FTIR spectrometer, in a range from 350 to 4000 cm^{-1}, with a maximum resolution of 1 cm^{-1}. Samples were prepared by placing a drop of the solution on a KBr pellet and then evaporating the solvent at room temperature. FTIR spectra on the powders were measured on pellets prepared by mixing the powders with KBr with a sample:KBr volume ratio of about 1:50.

UV−vis optical absorption spectra on the solutions were obtained on a Shimatzu (UV-2101 PC) spectrophotometer. The solutions were diluted in methanol before the measurement.

Electron paramagnetic resonance (EPR) spectra were performed on a Bruker EMX spectrometer working at the X-band frequency, equipped with a Oxford cryostat operating in the range of temperature 4−298 K. Modulation frequency was 100 kHz, modulation amplitude 5 gauss, microwave power 10 mW, where not differently indicated. The g and A values were calculated by simulation and fitting of the experimental spectra by using SIM 14S program[10] and with α,α′-diphenyl-β-picryl hydrazyl (DPPH) as reference.

X-ray photoelectron spectroscopy (XPS) analyses were performed with a PHI ESCA-5500 equipment working with the Al

(6) Epifani, M.; Alvisi, M.; Mirenghi, L.; Leo, G.; Siciliano, P.; Vasanelli, L. *J. Am. Ceram. Soc.* **2001**, *84*, 48–54.
(7) Epifani, M.; Imperatori, P.; Mirenghi, L.; Schioppa, M.; Siciliano, P. *Chem. Mater.* **2004**, *16*, 5495–5501.
(8) (a) Oyama, S. T.; Somorjai, G. A. *J. Phys. Chem.* **1990**, *94*, 5022–5028. (b) de Cruz, A. M.; Eon, J. G. *Appl. Catal., A: Gen.* **1998**, *167*, 203–213. (c) Reddy, B. M.; Ganesh, I.; Chowdhury, B. *Catal. Today* **1999**, *49*, 115–121. (d) Chen, Y.; Wachs, I. E. *J. Catal.* **2003**, *217*, 468–477. (e) Shimamura, T.; Okumura, K.; Nakagawa, K.; Ando, T.; Ikenga, N.-o.; Suzuki, T. *J. Mol. Catal. A: Chem.* **2004**, *211*, 97–102. (f) Hess, C. *Surf. Sci.* **2006**, *600*, 3695–3701. (g) Malleswara Rao, T. V.; Deo, G. *Ind. Eng. Chem. Res.* **2007**, *46*, 70–79. (h) Bautista, F. M.; Campelo, J. M.; Luna, D.; Luque, J.; Marinas, J. M. *Appl. Catal., A: Gen.* **2007**, *325*, 336–344.
(9) (a) Vuurman, M. A.; Wachs, I. E.; Hirt, A. M. *J. Phys. Chem.* **1991**, *95*, 9928–9937. (b) Tesser, R.; Maradei, V.; Di Serio, M.; Santacesaria, E. *Ind. Eng. Chem. Res.* **2004**, *43*, 1623–1633. (c) Herrera, J. E.; Ja Hun Kwak, J. H.; Jian Zhi Hu, J. Z.; Yong Wang, Y.; Peden, H. F. *Top. Catal.* **2006**, *39*, 245–255. (d) Zhao, C.; Wachs, I. E. *J. Phys. Chem. C* **2008**, 11363–11372.
(10) Lozos, G. P.; Hofman, B. M.; Franz, C. G. Quantum Chemistry Program Exchange, no. 65, 1973.

Kα radiation (1486.6 eV). The powders were fixed on the sample holder with a biadhesive film, giving them a certain amount of surface charging on all of the peak positions of the main narrow scan spectra acquired: V2p3/2, O1s, C1s, Cl2p. They were all properly corrected with respect to the adventitious C1s present on the surface with respect to the tabulated and literature value of 284.6 eV.

X-ray diffraction (XRD) measurements were performed on a Panalytical X'Pert PRO-MPD diffractometer working with the Cu Kα radiation ($\lambda = 1.5406$ Å) using a Bragg−Brentano geometry. For thin film measurements, the sample was tilted 2° to reduce the intensity of the silicon substrate. XRD measurements coupled with in situ heating steps were carried out using an alumina sample holder with an incorporated heater. The temperature was initially increased from room temperature to 200 °C in steps of 50 °C from room temperature, and subsequently increased in steps of 30 °C from 200 to 400 °C. A 10 °C/min heating rate was used to move from one temperature to another. The diffraction patterns were acquired at each selected temperature in the 10−100° 2θ range with a step time of 200 s and a step size of 0.017°. Synthetic air was flowed over the samples to reproduce the conditions of the static heat-treatments described above.

Thermogravimetry (TGA) and differential scanning calorimetry (DSC) were employed to investigate the thermal evolution of the V_2O_5 precursor, in nonisothermal condition. TGA measurements were carried out using a Mettler TGA/SDTA851e thermobalance, and DSC measurements were done using a DSC-822e Mettler Toledo analyzer. A sample mass of about 10 mg was heated to 600 °C in an open aluminum crucible at a rate of 5 °C/min, in a constant flow of 50 mL/h of synthetic air.

The morphology of the thin films and the powders was observed with a JEOL JSM6500F FEG scanning electron microscope.

High-resolution transmission electron microscopy (HRTEM) studies were carried out with a field emission gun microscope Jeol 2010F, which works at 200 kV and has a point-to-point resolution of 0.19 nm.

The gas-sensing tests on devices prepared with the V_2O_5 powders heat-treated at 500 °C were carried out using a standard configuration for resistive sensor measurement, with Pt-interdigitated electrodes and a Pt-resistive-type heater printed onto an alumina substrate. Sensors were prepared by depositing a mixture of the V_2O_5 powder with 1,2-propanediol onto interdigitated electrodes, and subsequently annealing at 400 °C for 1 h to burn the organic binder and to ensure sample adhesion to the alumina surface. The sensor devices were placed in a sealed chamber with a constant flux of 0.2 L/min of synthetic air into which the desired amount of test gases was mixed. Next, the sensor response was measured as the ratio of the sensor electrical resistance in the presence or absence of the target gas. It is defined as R_{air}/R_{gas} for reducing gases such as those tested in the present work, NH_3 and ethanol.

Results and Discussion

A. Preparation and Properties of the Starting Solutions. *i. Early Determination of the Main Species in Solution.* After water addition to the solvolyzed VCl_4 solution, no precipitation occurred, and the resulting solutions were stable for at least 1 year. On the other hand, color change was observed, as described in the Experimental Section, from the initial green to the final bright blue, at a rate increasing with the water amount. In practice, the color change was complete after 2 weeks for $r = 16$ and after 1 month for $r = 0$; in this latter case, it had begun 2 weeks after the initial solvolysis reaction. To understand the origin

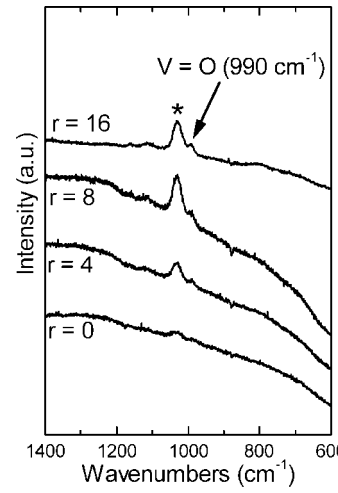

Figure 1. Raman spectra measured on solutions prepared with the indicated values of the H_2O:V molar ratio. The asterisk indicates a methanol band.

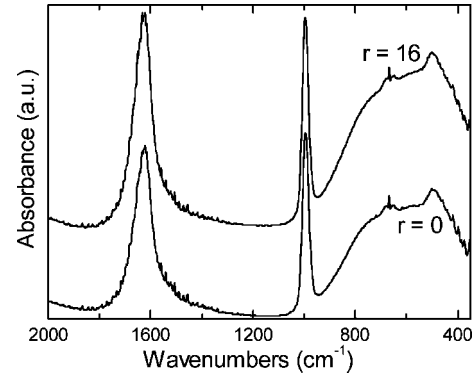

Figure 2. FTIR spectra measured on solutions prepared with the indicated values of the H_2O:V molar ratio. The spectra have been measured after the color change of the solutions was complete.

of the solutions' stability, the structure of the precursor was investigated in a stepwise approach, and we reasoned it as follows.

First, the observed colors are typical of complexes containing the vanadyl [$(V{=}O)^{2+}$] group.[11] In the Raman spectra of samples with various r values, shown in Figure 1, a strong methanol band (starred) dominates the signal, but a band is clearly observed at 990 cm^{-1} for all of the r values. FTIR spectra, reported in Figure 2 for samples analyzed after solvent evaporation, show a sharp band at 995 cm^{-1}. These vibrational features give strong evidence of the VO^{2+} presence.[12]

The easy formation of the vanadyl in the room temperature methanolysis of VCl_4 was indeed reported by Bradley et al.,[13] who had to control the reaction rate by the low temperature, to obtain the dichloride dialkoxide free from the oxychloride. A huge amount of spectral data was collected in the past concerning the VO^{2+} ion, so the next step of our investigation

(11) Cotton, F. A.; Wilkinson, G. *Advanced Inorganic Chemistry*, 5th ed.; Wiley: New York, 1988; p 286.
(12) Evans, J. C. *Inorg. Chem.* **1963**, *2*, 372–375.
(13) Bradley, D. C.; Multani, R. K.; Wardlaw, W. *J. Chem. Soc.* **1958**, 4647–4651.

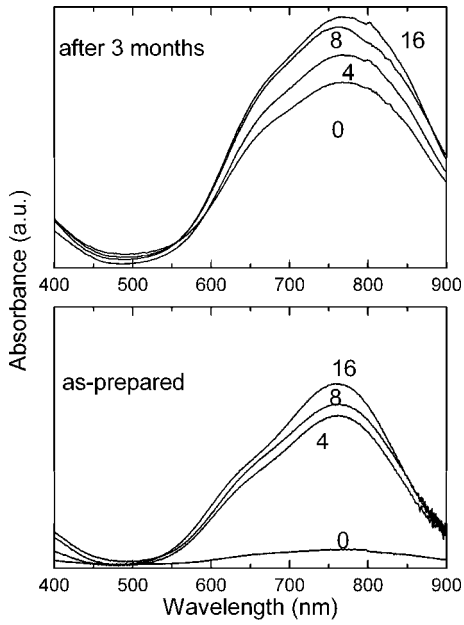

Figure 3. UV−vis spectra measured on the solutions prepared with the indicated r values in different stages of the aging process.

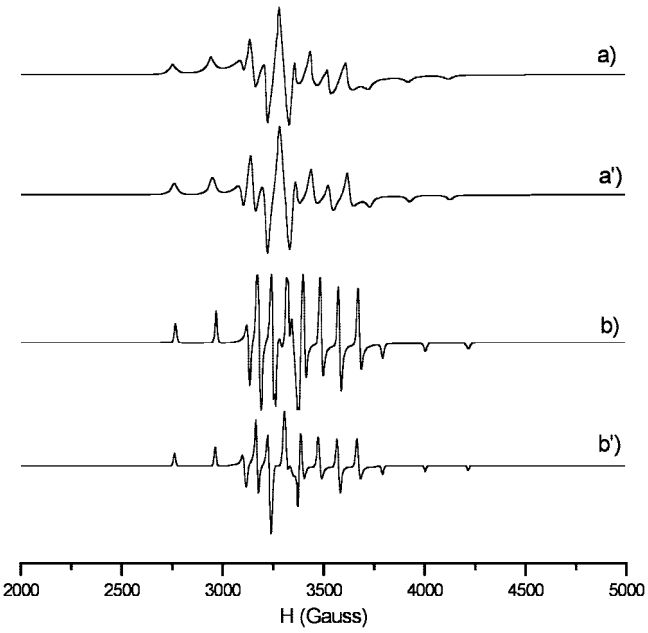

Figure 4. EPR spectra, recorded at 123 K, of (a) VCl_4 methanol solution ($r = 0$) and (b) VCl_4 methanol solution after water addition ($r = 16$); a′ and b′ are the simulated spectra.

was the determination of the symmetry and composition of the ligand field around it.

ii. Symmetry of the Vanadyl Environment. The most striking spectral feature was the color change and its water-dependent rate, so the optical spectra of solutions with different r values were recorded both on the as-prepared solutions and on those aged for 3 months. The results are shown in Figure 3 for the spectral region from 400 to 900 nm. The spectra in the high-frequency region are shown in Figure S1 (Supporting Information). In the 400−900 nm region, the as-prepared solution with $r = 0$ shows relatively weak absorptions in the visible region due to d−d transitions and strong bands in the UV region due to charge transfer absorptions (Figure S1). By increasing r, the intensity of the bands in the visible region increases, as well as the intensity of the absorption between 350 and 250 nm. After 3 months, for $r = 0$ the intensity in the visible region has become comparable with the higher r values, while for all r values the UV bands became very similar. The structure of the absorption curve in the visible region consists of two overlapped components: a main band at about 770 nm and a weaker component below 650 nm.

In the aged solutions, an increasing absorption appears on the lower energy flank, most probably indicating a third band. The change of color by water addition may be associated with the increased intensity of the bands in the interval 600−900 nm.

The optical properties of the vanadyl ion were extensively investigated by Ballhausen and Gray, who provided a classical account of the ion structure in terms of molecular orbitals.[14] The authors considered the $[VO(H_2O)_5]^{2+}$ ion having the C_{4v} symmetry of distorted octahedron, where four water molecules occupy the equatorial positions and the last one the remaining axial site. They predicted three d−d bands in the visible region, due to the $^2B_2 \rightarrow {}^2E$ and $^2B_2 \rightarrow {}^2B_1$ and $^2B_2 \rightarrow {}^2A_1$ transitions, in order of increasing energy. On the other hand, Selbin and co-workers[15] demonstrated that if the vanadyl symmetry decreases from the original C_{4v} to C_{2v}, further splitting of the ^2E levels results. However, this phenomenon was evidenced only at low temperature, while at room temperature broad bands in the same regions were observed. In our case, we have a similar band structure, so a symmetry lower than C_{4v} (like C_{2v}) is suggested. Moreover, the intensity of the d−d transitions varied with r and the aging time. This result suggests less forbidden d−d transitions, due to higher mixing of d orbitals with ligand orbitals or to mixing of d orbitals with p orbitals, due to distortion of the crystal field symmetry. This effect, in turn, can be due to the change from C_{2v} to even lower symmetries by substitution of methoxy with hydroxo group. To summarize, the addition of water to methanolized VCl_4 results in low symmetry vanadyl complexes. It was then necessary to get more insight about the composition of the vanadyl environment.

iii. Vanadyl Environment. To deeply understand the vanadyl coordination, we performed an EPR investigation parallel to the optical analysis. The EPR spectra, recorded at low temperature (123 K), on VCl_4 methanol solution before ($r = 0$) and after the addition of water ($r = 16$), are typical of a d^1 VO^{2+} group (Figure 4).[16] The magnetic parameters show slight differences for the two cases: $g_\perp(1) = 1.9231$, $g_{||}(1) = 1.9775$, $A_\perp(1) = 74.4$, $A_{||}(1) = 195.0$ in the methanol solution; $g_\perp(2) = 1.9347$, $g_{||}(2) = 1.9833$, $A_\perp(2) = 77.0$, $A_{||}(2) = 201.4$ after addition of water. The increase in the hyperfine coupling is attributable to the substitution of the alkoxo by the hydroxo group, which increases the unpaired electron density on the metal center.

(14) Ballhausen, C. J.; Gray, H. B. *Inorg. Chem.* **1962**, *1*, 111–122.

(15) (a) Selbin, J.; Ortolano, T. R.; Smith, F. J. *Inorg. Chem.* **1963**, *2*, 1315–1316. (b) Selbin, J. *Coord. Chem. Rev.* **1966**, *1*, 293–314. (c) Sacconi, L.; Campigli, U. *Inorg. Chem.* **1966**, *5*, 606–611.

(16) Davidson, A.; Che, M. *J. Phys. Chem.* **1992**, *96*, 9909.

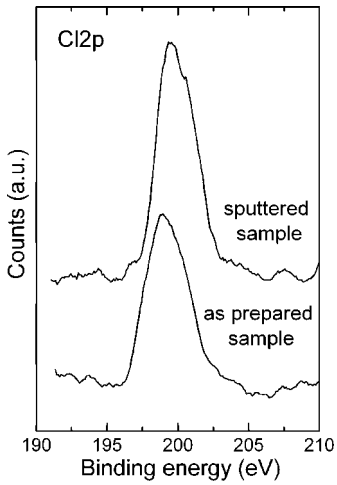

Figure 5. XPS spectra in the Cl2p region acquired on a thin film prepared with $r = 16$ and dried at 100 °C.

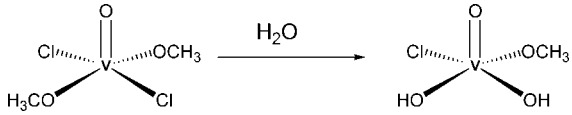

Figure 6. Schematic view of the evolution of the vanadium chloromethoxide upon hydrolysis, with the resulting final structure.

From the use of VCl_4 as a precursor, the presence of residual chlorine even after water addition may be expected, depending on the hydrolytic stability of the V−Cl bond. The Raman and IR spectra of pure VCl_4 were studied in detail in the past,[17] but the methanolysis strongly changes the symmetry of the vanadium environment, making it very hard to assess the presence of the V−Cl bonds by vibrational spectroscopy.

Instead, the presence of chlorine in our solutions was verified by XPS analysis on the as-prepared films ($r = 16$), dried at 100 °C. This is a fast analysis whose results are not obvious, because, depending on the metal cation, complete elimination of the chlorine ligands may occur even soon after the film deposition and drying.[18] The results are shown in Figure 5. The presence of residual chlorine is evident, even after sample sputtering, which excluded that Cl could be present only as surface accumulated residual.

Putting together all of these results, we conclude that upon initial methanolysis vanadyl complexes are formed with formula $[VOCl_x(OCH_3)_y]^{2-}$ ($x + y = 4$, $x = 2$ or 3). After water addition, hydrolysis of the methoxo and/or chloro ligands results in symmetry lowering and color change of the solutions. A structure example is shown in Figure 6.

It was important to investigate why even the solution with $r = 0$ was subjected to color changes: a common chemical feature emerged with the synthesis of chloroalkoxides of other elements. The explanation was first suggested by Bradley et al.,[13] who highlighted the alcohol reaction with the hydrochloric acid produced in the primary solvolysis reaction:

$$MeOH + HCl \rightarrow MeCl + H_2O$$

The actual presence of water in the solutions with $r = 0$ is indicated by the FTIR spectra of Figure 2, where a strong water band had been highlighted. For verifying the suggestion

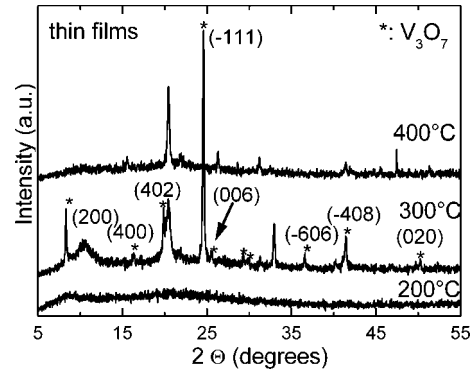

Figure 7. XRD patterns measured on thin films heat-treated at the indicated temperatures. The most intense peaks of the V_3O_7 phase are indexed in the 300 °C pattern.

by Bradley, we carried out a synthesis by dissolving silver nitrate in methanol before reaction with VCl_4, to hinder the previous reaction by chlorine elimination. After the reaction was carried out, the precipitated AgCl was filtered, and the resulting dark green solution was kept in a vial. No color change occurred in this case even after 2 months. This result shows that the green-to-blue transition in solutions with $r = 0$ is due to in situ formed water and confirms the fundamental role of water in reactions of the initial vanadyl complexes. Moreover, it results that in each chloroalkoxide synthesis the role of in situ formed water must be taken into account.

Definitely the stability of the VCl_4 methanol solution after the addition of water is due to the maintenance of the VO^{2+} group and of the residual chlorine ligands, both hindering further hydrolysis and condensation of the partially hydrolyzed precursor.

B. Formation and Structural Evolution of Thin Films and Powders. The low sol−gel polymerization functionality of the starting solutions is overcome during the spin-coating of the films by solvent evaporation. Very uniform films were obtained, without any strict control of the environment moisture, the residual chlorine preventing too fast condensation of vanadyl precursor. The same effect, more evident, was observed in the powder preparation: the initial drying at reduced pressure of the solutions only resulted in viscous dark oil, which finally condensed only upon further drying. The thermal evolution of these materials was first investigated by XRD. As indicated in the Experimental Section, all of the following investigations were carried out on materials prepared with $r = 16$.

The results are summarized in Figures 7 and 8 for thin films and powders, respectively. For clarity, only some patterns were reported in a selected range. The whole temperature sequences up to 500 °C in a broader 2Θ range are reported in the Supporting Information (Figures S2 and S3). Both powders and thin films are amorphous or display weak and broad peaks up to 200 °C. After heat-treatment at 300 °C, a mixture of the V_2O_5 phase with substoichiometric V_3O_7 was observed. After heat-treatment at 400 °C, only V_2O_5 was detected. V_2O_5 is constituted by penta-coordinated

(17) (a) Clark, R. J. H.; Hunter, B. K.; Mitchell, P. D. *J. Chem. Soc., Faraday Trans.* **1972**, *2*, 476–480. (b) Creighton, J. A.; Green, J. H. S.; Kynaston, W. *J. Chem. Soc. A* **1966**, 208–210.

(18) This occurs for MoO_3 (see ref 5) and WO_3 (unpublished results).

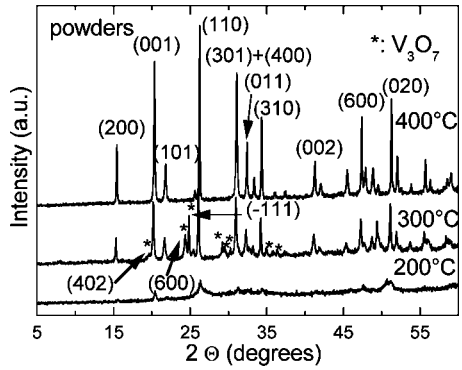

Figure 8. XRD patterns measured on the dried precursor powders heat-treated at the indicated temperatures. The peaks of the V_2O_5 phase are marked in the 400 °C pattern, while those of V_3O_7 are in the 300 °C pattern. For clarity, only the most intense peaks have been indexed.

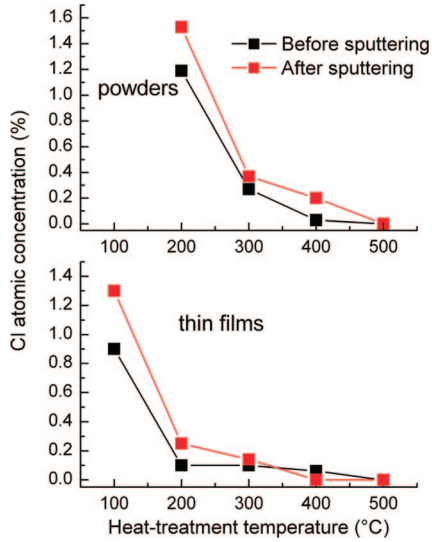

Figure 9. Chlorine atomic concentration deduced from XPS analysis on thin films and powders as a function of the heat-treatment temperature. The analyses were carried out both on surface and after Ar^{3+} sputtering.

V in distorted trigonal bipyramids or square pyramids, forming infinite layers.[19] The structure of V_3O_7 is constituted[20] by both penta- and hexa-coordinated vanadium in chains and strings of octahedra and trigonal bipyramids and square pyramids. Both V^{4+} and V^{5+} cations are present ($V_2^{5+}V^{4+}O_7$), the former being associated with octahedral sites and the latter with bipyramids. The structural difference between the two phases allows one to suppose that a reconstructive transition occurs when V_3O_7 is converted to V_2O_5. The reason for these transformations was indicated by the XPS analysis of the powders and thin films for evaluating residual chlorine. The analyses were carried out even after sample sputtering, for obtaining data related to the inner sample region. The results are reported in Figure 9.

Chlorine elimination occurred when the heat-treatment temperature changed from 200 to 300 °C. A detectable

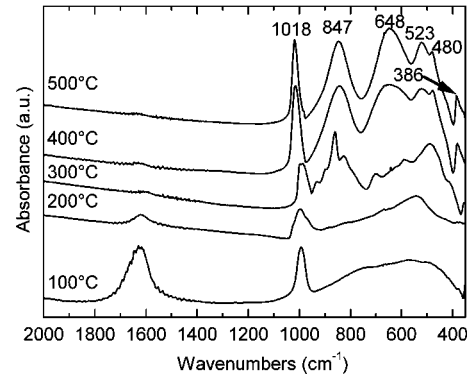

Figure 10. FTIR spectra measured on the V_2O_5 precursor powders heat-treated at the indicated temperatures in air.

chlorine atomic concentration was found even after heat-treatment at 300 °C, while after heat-treatment at 400 °C Cl disappeared from the samples. By comparing these results with the XRD patterns, it was concluded that chlorine delayed the formation of new V−O bonds up to 300 °C. When it was eliminated during heat-treatment at 300 °C, the resulting oxygen-deficient structure favored the formation of V_3O_7. For investigating more in detail the structural evolution of the sample, the XRD patterns were recorded with in situ heating of the sample, as described in the Experimental Section. Interestingly, the results, reported in the Supporting Information (Figure S4), show that the intermediate V_3O_7 formation is completely suppressed. Because an air flow was used in the analysis, this result was interpreted in terms of fast annealing of the oxygen deficiency induced by chlorine elimination. In the static heat-treatments used for the samples of Figures 7 and 8, there was no air flow, implying slower recovery of the oxygen stoichiometry. It must be finally noted that XPS measurements in the V2p region were not helpful for investigating the materials transformations, because the surface region systematically showed the prevalent presence of V(V), as shown in the Supporting Information (Figure S5). Only a very weak V(IV) component could be found after peak analysis. This phenomenon is due to the heat-treatment procedure in air, which easily oxidizes the surface layers up to the V(V) state. Indeed, in past papers on the XPS study of vanadium oxides,[21] this problem had already been described. Even the quantification of the V/O atomic ratio was not useful because, as shown in Table S1 of the Supporting Information, a strong oxygen excess was obtained.

Vibrational studies were carried out to establish a parallel with the XRD results. The IR and Raman spectra for powder samples are reported in Figure 10 and Figure S6 (Supporting Information), respectively. The peaks in the IR curves for the samples heat-treated at 500 °C were marked as a reference, and all were attributed to V_2O_5 modes, following early literature reports.[22] In the sequence of IR spectra, it is

(19) (a) Byström, A.; Wilhelmi, K.-A.; Brotzen, O. *Acta Chem. Scand.* **1950**, *4*, 1119–1130. (b) Bachmann, H. G.; Ahmed, F. R.; Barnes, W. H. *Z. Kristallogr.* **1961**, *115*, 110–131. (c) Enjalbert, R.; Galy, J. *Acta Crystallogr., Sect. C* **1986**, *42*, 1467–1469.

(20) (a) Andersson, S.; Galy, J.; Wilhelmi, K. A. *Acta Chem. Scand.* **1970**, *24*, 1473–1474. (b) Waltersson, K.; Forslund, B.; Wilhelmi, K.-A.; Andersson, S.; Galy, J. *Acta Crystallogr., Sect. B* **1974**, *30*, 2644–2652.

(21) (a) Mendialdua, J.; Casanova, R.; Barbaux, Y. *J. Electron Spectrosc. Relat. Phenom.* **1995**, *71*, 249–261. (b) Silversmit, G.; Depla, D.; Poelman, H.; Marin, G. B.; De Gryse, R. *J. Electron Spectrosc. Relat. Phenom.* **2004**, *135*, 167–175.

(22) (a) Gilson, T. R.; Bizri, O. F.; Cheetham, N. *J. Chem. Soc., Dalton Trans.* **1973**, *3*, 291–294. (b) Abello, L.; Husson, E.; Repelin, Y.; Lucazeau, G. *Spectrochim. Acta, Part A* **1983**, *39*, 641.

seen that in the as-dried precursors (100 °C) only the vanadyl stretching is observed, together with a broadband below 900 cm^{-1} and the water bending at about 1620 cm^{-1}. The well-developed vanadyl band simultaneously with the broad signal below 900 cm^{-1}, where the stretching modes of VO_2 and VO_3 units are expected, indicates partial polymerization of the starting vanadyl-containing species. Because only weak shoulders are seen where such modes are expected, the three-dimensional network is far from being built up, in agreement with the XRD results. The hindrance of the VO_2 and VO_3 units formation, in turn, further points to the presence of residual chlorine limiting the reactivity of the starting species. Upon further heating, water is completely desorbed and/or reacted with the vanadium precursor, as seen by the decrease of the band at 1620 cm^{-1}. The structural evolution of the precursor first continues by organization of the previous structure, as indicated by the broadening of the vanadyl band and by the appearance of a peak at about 520 cm^{-1} in the curve of the sample heat-treated at 200 °C. After heating at 300 °C, the structural evolution becomes discontinuous, in the sense that the curve of the 200 °C sample does not evolve smoothly toward that of the 400 °C heated sample, where the V_2O_5 structure is clearly observed. Instead, new peaks appear, parallel to the V_3O_7 peaks in the related XRD patterns.

For this reason, we attribute such peaks to the V_3O_7 phase, despite that no data are available about the vibrational properties of such phase, to the best of our knowledge. The "discontinuous" evolution of the IR spectra reinforces the previous hypothesis of a separate formation of V_3O_7 from V_2O_5. After heating at temperatures higher than 400 °C, only the V_2O_5 structure is present, in agreement with the XRD patterns. The evolution of the Raman spectra, shown in the Supporting Information, does not show relevant features, differently from the IR data. It is not clear whether this can be due to the low V_3O_7 content or to the eventually few Raman active modes of such phase.

EPR spectra, recorded at 123 K, of dried precursor and powders annealed at increasing temperatures (100 and 300 °C) are reported in Figure 11. In all samples, no signals of isolated vanadyl species are evident. Spectra of dried precursor and powders annealed at 100 °C show intense broad symmetric resonances centered at $g = 1.97$, with shape similar to that of dimeric $S = 1$ species and a narrow resonance, centered at the same field, which becomes more intense at high level of microwave power, attributable to a double quantum transition.[23] Although the lack of resolution does not allow one to distinguish the fine structure of the spectrum, the value of the zero field parameter ($D' =$ 400−500 gauss) is low, suggesting low dipolar contribution due to $V^{4+}-V^{4+}$ interaction of the vanadyl groups via bridging oxo and hydroxo groups in the dried precursor matrix. After the annealing at 300 °C, EPR spectra change and show a narrow (ΔH_{pp} 190 G) symmetrical line at $g =$ 1.95. The spectroscopic parameters are very similar to those

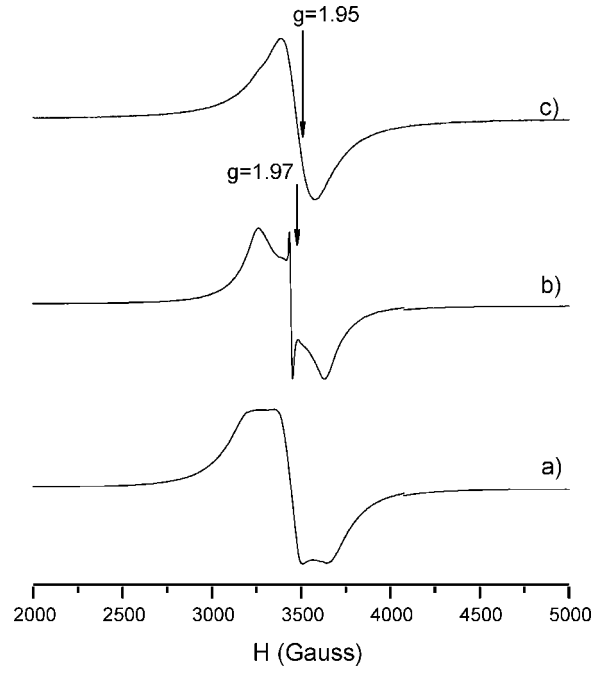

Figure 11. EPR spectra, recorded at 123 K, of (a) as-prepared dried precursor and of samples annealed (b) at 100 °C and (c) at 300 °C.

found for V^{4+} ions in a series of vanadium oxides,[24] where the high concentration of paramagnetic centers causes an exchange-narrowing of EPR lines. This is in agreement with the suggested formation of V_3O_7 phase, where a large amount of V^{4+} ions, surrounded by six oxygen atoms, are located in octahedra arranged as linear and double chains.[25] After the annealing at 400 and 500 °C, the amount of paramagnetic species is negligible, as expected after V_2O_5 formation.

The role of residual chlorine in the transformation from the V_3O_7 to the final V_2O_5 phase was investigated also by thermal analyses in air, whose results are shown in Figure 12. Up to 250 °C, there is a huge mass loss due to endothermic phenomena, interpreted as the elimination of water, also generated by condensation reactions, and the elimination of chlorine, this latter phenomenon attributed to the higher temperature peaks. After 300 °C, the TG curve is flattened, while very intense DSC exothermic peaks were observed. If the amplified TG trace in the inset is observed, a mass gain is evidenced, which assesses the oxidation of the precursor.

So, after 300 °C, the oxygen defects due to the previous chlorine elimination are removed, and the reaction product undergoes phase transition to V_2O_5, resulting in the exothermic peaks at high temperatures. From the TG data, the gain of the O/V atomic ratio was calculated in the region after 300 °C. Even supposing an initial ratio of 2.33, corresponding to the extreme case of pure V_3O_7 before the oxygen gain step, a final value of 2.42 was obtained, in good agreement with the expected increase for the transition to V_2O_5. The interpretation of the thermal analyses is in agreement with the results of previous

(23) (a) Wertz, J. E.; Bolton, J. R. *Electron Spin Resonance*; McGraw Hill: New York, 1972; p 292. (b) Pilbrow, J. R. *Transition Ion Electron Paramagnetic Resonance*; Clarendon Press: Oxford, 1990; p 265.

(24) Occhiuzzi, M.; Cordischi, D.; Dragone, R. *J. Solid State Chem.* **2005**, *178*, 1551.

(25) Nishihara, H.; Ueda, Y.; Kosuge, K.; Yasuoka, H.; Kachi, S. *J. Phys. Soc. Jpn.* **1979**, *47*, 790.

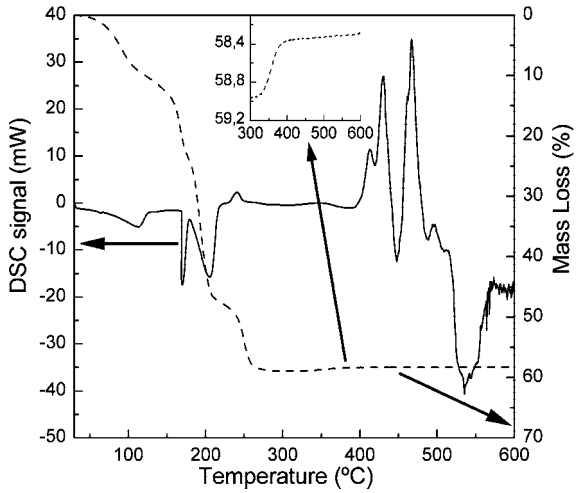

Figure 12. DSC/TG curves measured on the dried V_2O_5 precursor in air atmosphere. The inset shows the enlargement of the DSC curve above 300 °C.

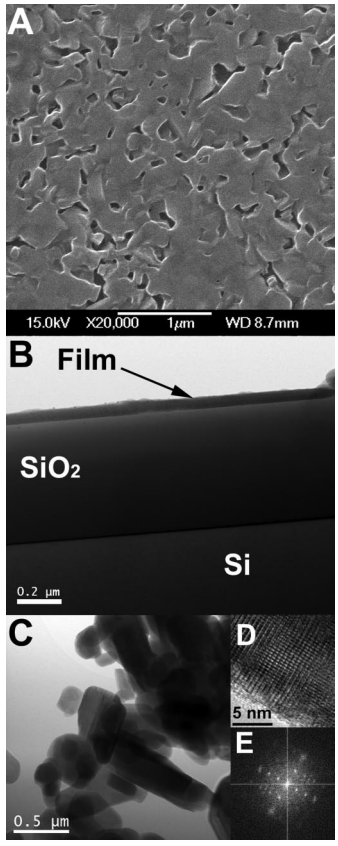

Figure 13. FE-SEM image of a V_2O_5 thin film heat-treated at 500 °C (A), general view TEM image of a thin film heat-treated at 300 °C (B), general view TEM micrograph of a powder heat-treated at 500 °C (C), HRTEM detail of a VO_2 nanocrystal in the same sample (D), and related power spectrum (E).

structural and vibrational investigations, and further shows the role of the V−Cl bond in determining the peculiarities of the process.

C. Morphology of Thin Films and Powders. The morphological features of the prepared materials were studied by both scanning and transmission electron microscopy, and some significant results are summarized in Figure 13. The film with $r = 16$ and heat-treated at 500 °C has a porous appearance when observed by SEM (Figure 13A), characterized by overlapped lamellar structures, which is in agreement with the layered structure of V_2O_5.

TEM characterizations were carried out on the film heat-treated at 300 °C, to investigate the two vanadium oxide phases. The general view TEM micrograph, reported in Figure 13B, shows that the film has a very uniform thickness over a long length scale. Unfortunately, no other structural details could be obtained by HRTEM, because the samples were reduced under the TEM beam, to such an extent that even elemental V nanocrystals were observed. This phenomenon has already been reported[26] and was also encountered when observing the powder samples. The morphology of the samples is shown in Figure 13C, where large crystals are observed, in agreement with the peak width in the XRD patterns of Figure 8. As an example of the underbeam reduction, in Figure 13D a high-resolution image is shown of a region with VO_2 composition, as shown in the power spectrum in Figure 13D (the related indexing is shown for clarity in the Supporting Information, Figure S7).

D. Sensing Properties of V_2O_5 Powders. The V_2O_5 powders heat-treated at 500 °C were used for fabricating thick film-based gas sensors, as described in the Experimental Section. This choice was dictated by our interest in applying metal oxides in gas sensing systems, and V_2O_5 has already been shown to be a potential candidate for the detection of various gases such as ethanol and amines.[27]

The resulting devices were characterized by remarkable conducting properties, with base resistance of the order of the kΩ. This feature limited the test temperatures to about 300 °C, which anyway is sufficient to detect a broad range of gas concentrations. In Figure 14 are shown the dynamic response curves, related to ethanol and ammonia sensing. The tested concentrations ranged from 50 to 500 ppm for both gases. The ammonia dynamic response curve has the typical features of those reported for reducing gases: by increasing the operating temperature, the electrical resistance decreases upon sensor exposure to the gas. The base resistance decreases with increasing the operating temperature, as expected for an n-type semiconductor: in this temperature range, the electrical conduction in V_2O_5 is due to electronic transport.[28] It can be noted that, after gas removal, the recovery of the base signal is complete, for each concentration and operating temperature.

The behavior for ethanol is qualitatively similar, but the signal is less regular than that of ammonia. From 50 to 200 ppm, the response increases from 175 to 225 °C, while for 500 ppm there is a saturation of the response already at 225 °C. Next, for 500 ppm at 250 °C, and for all concentrations at 275 °C, the response decreases. Finally, at 300 °C, the

(26) Su, D. S.; Wieske, M.; Beckmann, E.; Blume, A.; Mestl, G.; Schlögl, R. *Catal. Lett.* **2001**, *75*, 81–86.
(27) (a) Schilling, O.; Colbow, K. *Sens. Actuators, B* **1994**, *21*, 151–157. (b) Raible, I.; Burghard, M.; Schlecht, U.; Yasuda, A.; Vossmeyer, T. *Sens. Actuators, B* **2005**, *106*, 730–735. (c) Liu, J.; Wang, X.; Peng, Q.; Li, Y. *Adv. Mater.* **2005**, *17*, 764–767. (d) Serier, H.; Achard, M. F.; Babot, O.; Steunou, N.; Maquet, J.; Livage, J.; Leroy, C. M.; Backov, R. *Adv. Funct. Mater.* **2006**, *16*, 1745–1753. (e) Leroy, C. M.; Achard, M. F.; Babot, O.; Steunou, N.; Massé, P.; Livage, J.; Binet, L.; Brun, N.; Backov, R. *Chem. Mater.* **2007**, *19*, 3988–3999.
(28) Gillis, E.; Boesmann, E. *Phys. Status Solidi* **1966**, *14*, 337–347.

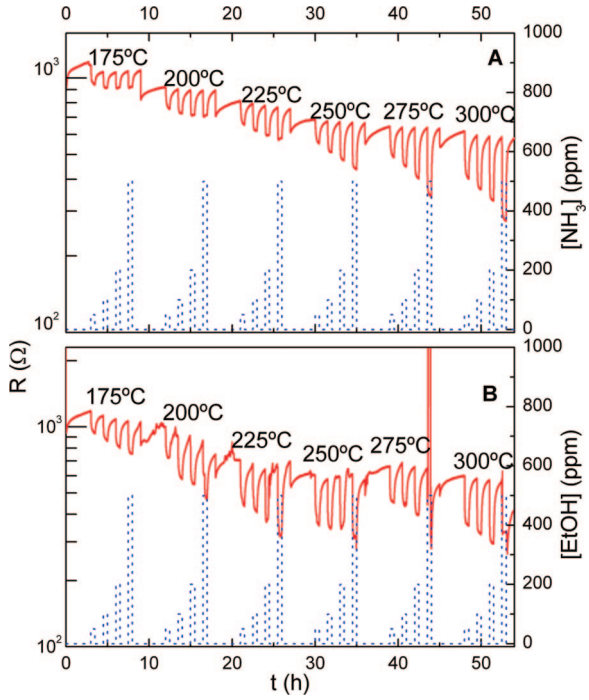

Figure 14. Dynamic response curves of sensors prepared with V_2O_5 powders heat-treated at 500 °C. In the upper panel (A), the results are reported for ammonia, while in panel B the data are for ethanol.

response is the highest. This oscillating behavior is not reported in other papers about V_2O_5 sensors, because lower operating temperatures were used.[27] In supported form, V_2O_5 is a known catalyst for ethanol oxidation to acetaldehyde at low temperatures,[29] but it was reported[8a] that the reaction product changes over the same temperature range where we observe the oscillating sensor response. In particular, the conversion products were mainly acetaldehyde and acetic acid at 490 K, while at 570 K a substantial production of ethylene was observed. On this basis, we propose that the sensors response in ethanol sensing is dictated by a change of the reaction mechanism when the operating temperature crosses a critical range around 250 °C. The calibration curves are reported in Figure 15, where the sensor response is plotted versus the gas concentration for various operating temperatures. The response of the sensor is defined as R_0/R_{GAS}, where R_0 and R_{GAS} are the electrical resistances in pure air and in the test gas, respectively. The responses follow the typical power laws for chemoresistive sensors,[30] but the exponents deduced from the plots follow different trends. In particular, for ammonia there is a regular increase from 0.02 at 200 °C to 0.15 at 275 °C (data for all temperatures are reported in the Supporting Information, Table S2). This is an indication that at lower temperatures a different mechanism could be operative, which is not surprising for ammonia, usually detected at high operating temperatures (300−400 °C). In the case of ethanol, an oscillating behavior is seen, with the slope soon rising from 0.1 at 175 °C to 0.2

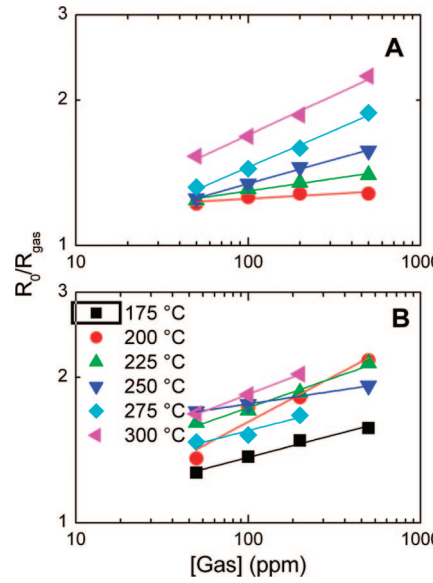

Figure 15. Calibration curves for ammonia (A) and ethanol (B).

at 200 °C, then decreasing at 250 °C, and again increasing at 300 °C. This result reinforces the hypothesis of different, overlapping mechanisms. The response values in Figure 15 show that it is possible to detect the tested gases over a broad concentration range. Moreover, more stable and reliable signal was obtained with respect to preliminary tests carried out with alkoxide-derived powders, most probably due to the less evident aggregation of the powders in the case of the chloroalkoxide-derived material.

Conclusions

For preparing V_2O_5 thin films and powders, a precursor can be easily synthesized from VCl_4, based upon sequential methanolysis and hydrolysis. The precursor is characterized by remarkable stability, allowing easy deposition of uniform thin films in the absence of a strict environmental control. The precursor stability was shown to derive from its molecular structure, based on chlorine-containing vanadyl complexes, characterized by limited sol−gel functionality. Complete chlorine elimination occurs after heat-treatment at 400 °C, which also converts the structure to the stable V_2O_5 phase. At lower temperatures, substoichiometric V_3O_7 was found, which was shown to be induced by the presence of residual chlorine. As an example of application, the powders were used for the convenient preparation of gas sensing devices, showing reliable response to reducing gases (NH_3, EtOH) over an extended range of concentrations.

Acknowledgment. We thank the XRD, Raman, FTIR, XPS units, and the platform of polymorphism and calorimetry for TGA-DSC measurements of the Serveis Científico-Tècnics of the Universitat de Barcelona.

Supporting Information Available: Further optical absorption, Raman and EPR spectra, XRD patterns, XPS spectra and quantification data, TEM images, and sensing data (PDF). This material is available free of charge via the Internet at http://pubs.acs.org.

CM803242M

(29) Kilos, B.; Bell, A T.; Iglesia, E. *J. Phys. Chem. C* **2009**, *113*, 2830–2836, and references therein, beyond those quoted in refs 8 and 9.
(30) Yamazoe, N.; Shimanoe, K. *Sens. Actuators, B* **2008**, *128*, 566–573.